

Chemical Science

Accepted Manuscript

This article can be cited before page numbers have been issued, to do this please use: J. Zhou, Q. Huang, Y. Lv, Z. Song, L. Gan and M. Liu, *Chem. Sci.*, 2026, DOI: 10.1039/D5SC08853D.



This is an Accepted Manuscript, which has been through the Royal Society of Chemistry peer review process and has been accepted for publication.

Accepted Manuscripts are published online shortly after acceptance, before technical editing, formatting and proof reading. Using this free service, authors can make their results available to the community, in citable form, before we publish the edited article. We will replace this Accepted Manuscript with the edited and formatted Advance Article as soon as it is available.

You can find more information about Accepted Manuscripts in the [Information for Authors](#).

Please note that technical editing may introduce minor changes to the text and/or graphics, which may alter content. The journal's standard [Terms & Conditions](#) and the [Ethical guidelines](#) still apply. In no event shall the Royal Society of Chemistry be held responsible for any errors or omissions in this Accepted Manuscript or any consequences arising from the use of any information it contains.

Highly Zincophilic-Hydrophobic Polyzwitterionic Hydrogel Electrolyte Enabled by Strong Electronegative Sulfobetaine-Carboxyl Motifs for Ultrastable Zinc-Ion Batteries

View Article Online
DOI: 10.1039/D5SC08853D

Received 00th April 20xx,
Accepted 00th April 20xx

DOI: 10.1039/x0xx00000x

Jia Zhou,^a Qi Huang,^d Yaokang Lv,^e Ziyang Song,^{b*} Lihua Gan,^{a,*} Mingxian Liu^{a,*}

Polyzwitterionic hydrogel electrolytes with good anionic affinity and well-aligned Zn²⁺ deposition effect are regarded as potential alternatives for propelling zinc-ion batteries (ZIBs). However, their hydrophilic molecular chains show relatively low zincophilicity and easily transfer H₂O molecules to the Zn surface, resulting in interfacial Zn corrosion and dendrites. Here we design highly zincophilic-hydrophobic polyzwitterionic hydrogel electrolyte (SC-PAM) via the crosslinking of zwitterionic sulfobetaine and carboxyl-rich carboxylated chitosan for ultrastable ZIBs. The zincophilic –SO₃[–] motifs of zwitterionic sulfobetaine in SC-PAM afford highly Zn²⁺-selective migration channels and homogenize Zn²⁺ flux with a high transference number of 0.90. Meanwhile, strong electronegative carboxyl groups (C=O) in carboxylated chitosan strongly anchor H₂O molecules via rich H-bonding interactions to establish a hydrophobic interfacial layer, which shields direct contact between H₂O solvent and Zn anode to avoid Zn corrosion. As a consequence, Zn||SC-PAM||Cu cell liberates a high average coulombic efficiency of 99.7% during 7600 cycles, while Zn||SC-PAM||Zn cell shows ultrastable cycling exceeding 7500 hours. Significantly, SC-PAM can be further leveraged to design state-of-the-art Zn||SC-PAM||V₂O₅ full battery with high capacity (372 mAh g^{–1}), large-current tolerance (15 A g^{–1}), and ultralong cycle life (5000 cycles). This work extends the structural engineering landscape of zincophilic-hydrophobic polyzwitterionic hydrogel electrolytes for advanced ZIBs.

Introduction

Aqueous zinc-ion batteries (ZIBs) have been proven to be attractive solutions for large-scale energy storage applications because their intrinsic advantages including high safety, low cost, and environmental compatibility.^{1–3} A key advantage of ZIBs arises from the Zn metal anode, which exhibits a low redox potential (–0.76 V vs. SHE), a high theoretical capacity (820 mAh g^{–1}), and excellent aqueous compatibility.^{4, 5} Despite the above merits, ZIBs still face fundamental challenges with several critical technical issues, which include dendrite growth, Zn corrosion reaction and hydrogen evolution reaction (HER).^{6–8} These issues originate from the undesirable interfacial reactions between Zn anodes and aqueous electrolytes.^{9–11} Although aqueous electrolytes offer high ionic conductivity suitable for high-power output, a large amount of free water molecules would accelerate HER, leading to poor interfacial stability. In contrast, non-aqueous electrolytes can effectively suppress HER and enhance low-temperature performance, but their practicality is limited by significantly reduced ionic conductivity and

high interfacial impedance.^{12–14} Thus, there is an urgent need to design new-type electrolytes that can protect the Zn anode from water-induced corrosion while simultaneously delivering enhanced Zn²⁺ ion transport kinetics.

Hydrogel electrolytes have garnered considerable attention because they integrate the high ionic conductivity of aqueous electrolytes and the low volatility of organic systems, along with the ability to form conformal interfacial contact through flexible polymer networks.^{15–17} Compared to conventional aqueous electrolytes, the restricted water environment within hydrogel electrolytes could confer better Zn anode cyclability.^{18, 19} Nevertheless, their practical application still faces challenges, such as sluggish Zn²⁺ ions migration kinetics and inefficient desolvation of hydrated Zn²⁺ ions, which limit the effectiveness of inhibitory effect.^{20, 21} Recently, researchers have developed polycation or polyanion-functionalized hydrogel electrolytes to overcome these limitations. Specifically, the positive electric field present in polycationic hydrogel electrolytes effectively immobilizes anions to enhance Zn²⁺ ion mobility and promote oriented Zn deposition, thereby inhibiting dendrite growth and mitigating tip effects.^{22, 23} Nevertheless, the hydrophilic segments of polycationic hydrogel electrolytes still struggle to effectively suppress water-induced side reactions. In contrast, polyanionic hydrogel electrolytes with zincophilic groups facilitate homogeneous Zn²⁺ ion transport and exhibit improved structural robustness.^{24, 25} However, excessive strong anionic interactions restrict the migration kinetics of Zn²⁺ ions.

To conquer the shortcomings of polycationic and polyanionic hydrogel electrolytes and leverage their relative functional advantages, polyzwitterionic hydrogel electrolytes have been developed, which liberate well-defined anion/cation migration

^a Shanghai Key Lab of Chemical Assessment and Sustainability, School of Chemical Science and Engineering, Tongji University, 1239 Siping Rd., Shanghai, 200092, P. R. China. *E-mail: ganlh@tongji.edu.cn; liumx@tongji.edu.cn

^b State Key Laboratory of Pollution Control and Resource Reuse, College of Environmental Science and Engineering, Advanced Research Institute, Tongji University, 1239 Siping Rd., Shanghai, 200092, P. R. China. *E-mail: songziyang@tongji.edu.cn

^c State Key Laboratory of Cardiovascular Diseases and Medical Innovation Center, Shanghai East Hospital, School of Medicine, Tongji University, 150 Jimo Rd., Shanghai 200120, P. R. China

^d Institute for Electric Light Sources, School of Information Science and Technology, Fudan University, 220 Songhu Rd., Shanghai 200438, P. R. China.

^e College of Chemical Engineering, Zhejiang University of Technology, 18 Chaowang Rd., Hangzhou 310014, P. R. China.



channels via electrostatic interactions between electropositive and electronegative groups.^{26–28} Polyzwitterionic hydrogel electrolytes thus promote rapid Zn^{2+} migration and homogenize Zn^{2+} flux to achieve well-aligned Zn deposition, leading to stable electrochemical process during the operation of ZIBs.^{29–31} As an example, Qiu group prepared sulfobetaine-functionalized polyzwitterionic hydrogel electrolytes to facilitate rapid ions migration with a high Zn^{2+} transference number of 0.84.³² $\text{Zn}||\text{Zn}$ battery thus exhibited stable cycling for 400 h at 2 mA cm^{-2} and $\text{Zn}||\text{Cu}$ battery maintained an average coulombic efficiency of 99.4% over 700 cycles. These results broaden the design horizons of polyzwitterionic hydrogel electrolytes for efficient ZIBs. Despite significant progress, polyzwitterionic chains with weak-electronegative sulfonate components are generally hydrophilic and can transport water molecules to directly contact Zn surface, which triggers the growth of Zn dendrites and parasitic side reactions over extended cycling. Thus, attempts are still required for further success in unlocking the intrinsic functional limitations of polyzwitterionic hydrogel electrolytes, thereby achieving better zincophilicity and hydrophobicity towards interfacial corrosion-resistant and dendrite-free Zn anodes for superior ZIBs.

In this work, we design a highly zincophilic-hydrophobic polyzwitterionic hydrogel electrolyte (SC-PAM) to guide uniform Zn^{2+} flux and effectively suppress Zn corrosion, thereby significantly enhancing the stability of Zn anodes. SC-PAM was fabricated through the crosslinking of zwitterionic sulfobetaine and carboxyl-rich carboxylated chitosan. The zincophilic $-\text{SO}_3^-$ functional groups of zwitterionic sulfobetaine in SC-PAM provide selective Zn^{2+} transport channel and promote uniform Zn^{2+} deposition with a high transference number of 0.90. In addition, the strongly electronegative carboxylated chitosan in SC-PAM forms a hydrophobic layer on Zn anode surface through H-bonding interactions, which prevents the Zn anode from direct water contact and efficiently restricts water molecule activity,

thereby inhibiting water-induced corrosion. Consequently, $\text{Zn}||\text{SC-PAM}||\text{Cu}$ cell demonstrates a average coulombic efficiency as high as 99.7% over 7600 cycles, while $\text{Zn}||\text{SC-PAM}||\text{Zn}$ cell achieves excellent cyclability exceeding 7500 hours. Besides, SC-PAM can be further leveraged to design advanced $\text{Zn}||\text{SC-PAM}||\text{V}_2\text{O}_5$ full battery with high capacity and cycling stability among previously reported batteries of the same type. These findings give new insights into the design of zincophilic-hydrophobic polyzwitterionic hydrogel electrolytes and stand for a good starting point for advanced ZIBs.

Results and Discussion

The electrochemical mechanism of zincophilic-hydrophobic SC-PAM is shown in Fig. 1. Specifically, the conventional polyacrylamide (PAM) hydrogel electrolyte exhibits inhomogeneous charge distribution on Zn anode surface, and faces the high desolvation energy of hydrated Zn^{2+} ions during repeated plating/stripping processes (Fig. 1a), leading to Zn corrosion and uncontrolled dendritic growth. In contrast, the incorporation of [2-(methacryloyloxy)ethyl]dimethyl-(3-sulfopropyl) (MDS, zwitterionic sulfobetaine) into PAM skeleton (denoted as S-PAM) immobilizes anionic carriers, effectively facilitating rapid Zn^{2+} migration and homogenizing the interfacial electric field, which ultimately suppresses Zn dendrites growth (Fig. 1b). However, the inherent hydrophilicity of polymeric chains of S-PAM permits water molecules to direct exposure to Zn anode, leading to Zn corrosion and gradually accelerating the formation of dendrites during long-term cycling. Significantly, SC-PAM are designed by the crosslinking of zwitterionic MDS and carboxyl-rich carboxylated chitosan (CC) as the polyzwitterionic hydrogel electrolyte for ZIBs. The zincophilic $-\text{SO}_3^-$ groups of zwitterionic sulfobetaine in SC-PAM are expected to

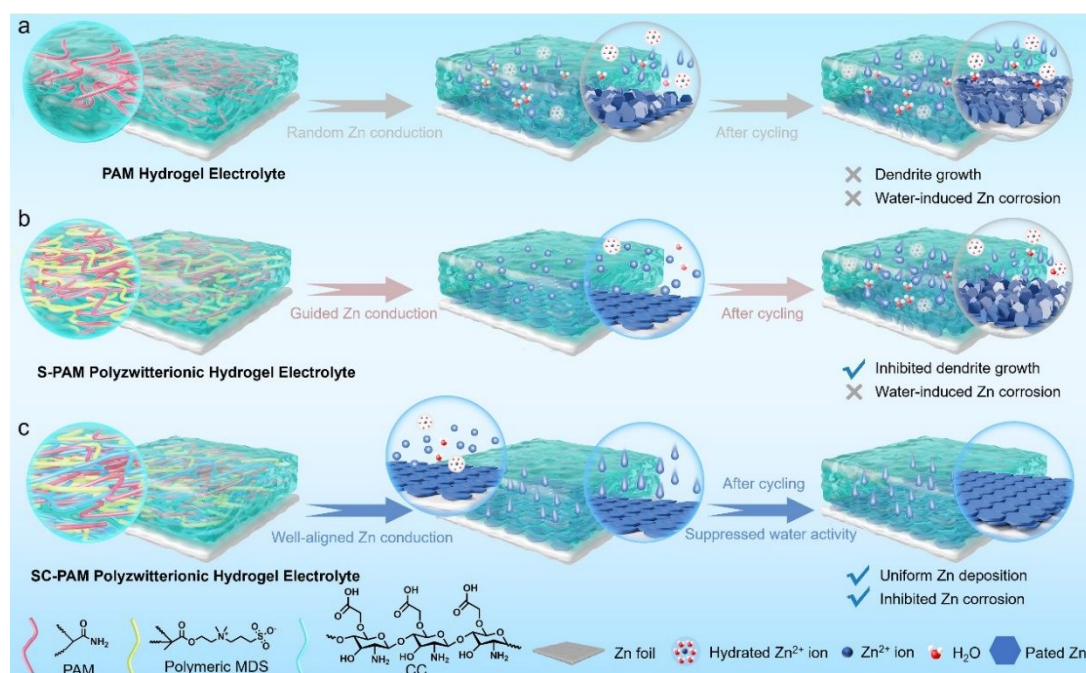


Fig. 1 Schematic illustration of the effects of (a) conventional PAM, (b) S-PAM and (c) SC-PAM hydrogel electrolytes on inhibiting Zn corrosion and dendrite formation.



provide selective Zn^{2+} transport pathways and boost uniform Zn^{2+} deposition (Fig. 1c). Meanwhile, the strongly electronegative carboxylated chitosan in SC-PAM can form a hydrophobic layer on Zn anode surface through H-bonding interactions, which is beneficial for preventing the Zn anode from direct water contact and efficiently restricting water molecule activity, thereby inhibiting water-induced corrosion to greatly improve the Zn anode cyclability.

The structure and composition of SC-PAM polyelectrolyte were probed by Fourier-transform infrared (FT-IR) spectroscopy and X-ray photoelectron spectroscopy (XPS). The characteristic peaks at 1025 and 1400 cm^{-1} could be observed, corresponding to C–OH and O–C=O groups for CC, respectively. The characteristic peaks at 1039 and 1190 cm^{-1} were assigned to S=O and $-\text{SO}_3^-$ groups for MDS (Fig. 2a and Fig. S1†).^{33, 34} In addition, XPS spectra show C 1s characteristic peaks of C–C, C–O/C–N and C=O (Fig. 2b and Fig. S2a†), and O 1s peaks of C–O and C=O (Fig. 2c and Fig. S2b†).³⁵ In addition, X-ray diffraction patterns of four hydrogel electrolytes show broad diffraction peaks centered at 27° , indicating the typical amorphous and non-crystalline polymer structures (Fig. 2d). This disordered feature facilitates the migration of ions along the polymeric chains.²³

Scanning electron microscope (SEM) images clearly show the smooth and flat surface of SC-PAM (Fig. 2e and Fig. S3†), along

with the homogeneous distribution of C, N, O, and S elements confirmed by the energy dispersive spectroscopy (EDS, Fig. 2f). The freeze-dried SC-PAM hydrogel electrolyte shows a porous three-dimensional network structure (Fig. S4a†) with the homogeneous distribution of C, N, O, and S elements (Fig. S4b†), which can serve as efficient ion-transport channels to facilitate fast Zn^{2+} migration. According to the electrochemical impedance spectra (Fig. 2g), the calculated ionic conductivity of SC-PAM is 8.54 mS cm^{-1} at room temperature, which is much higher than those of S-PAM, C-PAM and S-PAM ($0.815\text{--}3.05 \text{ mS cm}^{-1}$). The ion migration channels formed by zwitterionic groups in SC-PAM facilitate ions transport, and the polar carboxyl groups with strong electronegativity further enhance the conduction of Zn^{2+} ions (Fig. 2h). Moreover, the Zn^{2+} transference number was measured by using the chronoamperometry (CA) test. Compared with S-PAM, C-PAM and S-PAM ($0.52\text{--}0.74$), the Zn^{2+} transference number (t^+) of SC-PAM is as high as 0.9, reflecting its superior Zn^{2+} migration capability (Fig. 2h, Fig. S5 and 6†). The increase in Zn^{2+} transference number can be attributed to the polar carboxyl and sulfonic acid groups in SC-PAM interacting with cations, thereby optimizing the transport behavior of Zn^{2+} .^{26, 29} The electrochemical stability of SC-PAM as

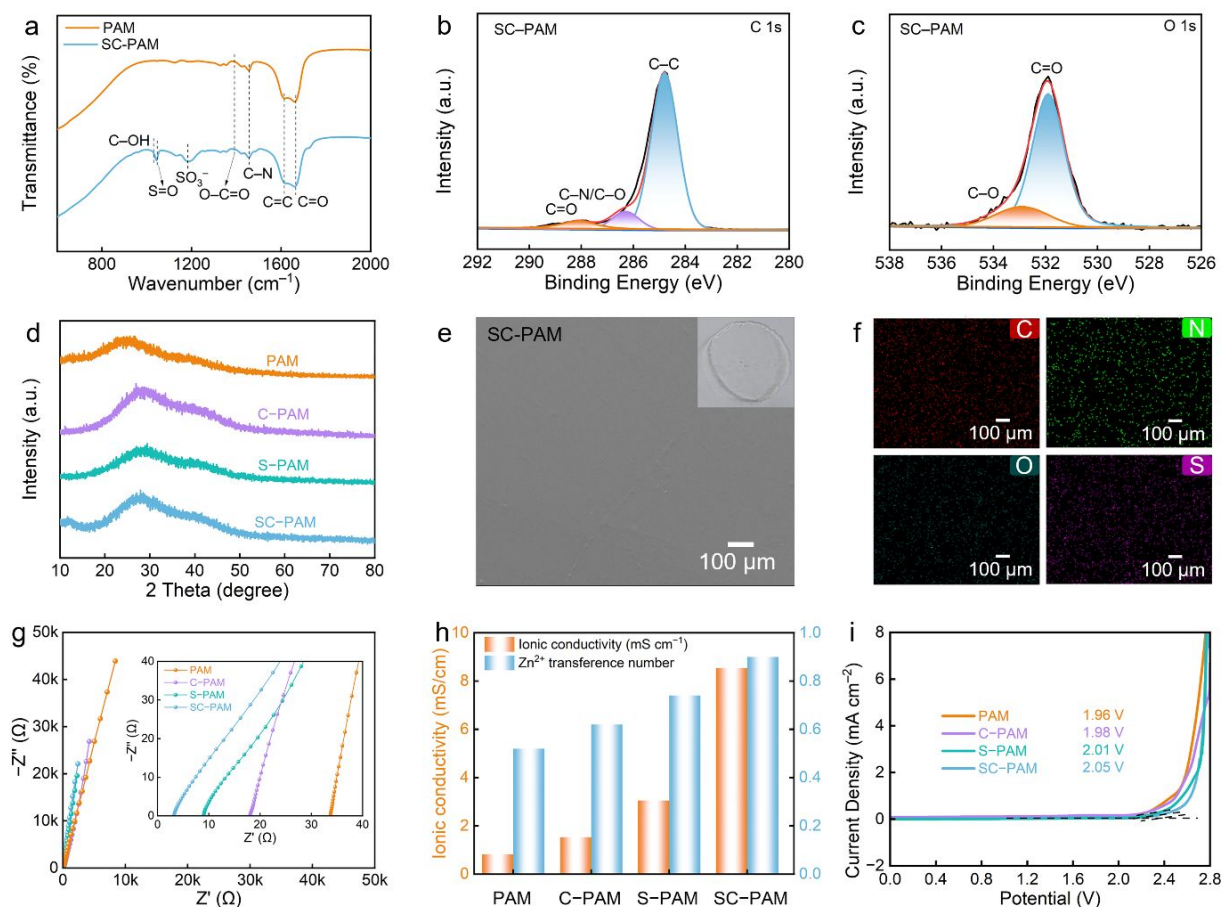


Fig. 2 Structural characterizations of S-PAM, C-PAM, S-PAM and SC-PAM hydrogel electrolytes. (a) FT-IR spectra. (b, c) XPS spectra of SC-PAM. (d) XRD patterns. (e) SEM image and (f) EDS images of SC-PAM (inset shows optical photo of SC-PAM). (g) EIS spectra. (h) The bar chart of ionic conductivity and Zn^{2+} transference number. (i) Linear sweep voltammetry.



the electrolyte in Zn||stainless steel cell was studied via linear sweep voltammetry measurement. As expected, SC-PAM possesses a broad electrochemical stable window of ~ 2.05 V, surpassing those of those of PAM (1.96 V), C-PAM (1.98 V), and S-PAM (2.01 V) due to suppressed water activity (Fig. 2i).³³

To investigate the influence of CC and MDS on solvation structure of SC-PAM, molecular dynamics (MD) simulations were conducted. Radial distribution functions (RDFs) and coordination numbers (CN) are utilized to illustrate the specific solvation structure of Zn^{2+} ions. The RDFs reveal that $\text{Zn}^{2+}\text{-O}$ in H_2O possesses a first solvation shell radius of ~ 1.975 Å, while the solvation shell radius of $\text{Zn}^{2+}\text{-O}$ in OTf^- is ~ 1.725 Å. The CN decreases from 5.61 to 5.19 (Fig. 3a–c and Fig. S7–S9†). Meanwhile, the number of H-bonds between water molecules was quantified in S-PAM, C-PAM, S-PAM and SC-PAM. The H-bonds number in SC-PAM is significantly lower than other hydrogel electrolytes (Fig. 3d), indicating that more water molecules are confined in SC-PAM.

The interaction between SC-PAM and water molecules was investigated by deconvoluting the broadband O–H stretching vibration bands in Raman spectra and FT-IR spectra using Gaussian functions, to reveal three distinct states of water molecules (Fig. 3e and f): I) Bound water (BW) at 3253 cm^{-1} , which originates from strongly H-bonding water molecules; II) Intermediate water (IW) at 3451 cm^{-1} associated with disrupted H-bonding and partial hydration networks; and III) Free water (FW) at 3624 cm^{-1} which represents unbound monomers, dimers, or trimers. The proportion of FW in SC-PAM is subsequently reduced, indicating that the

incorporation of hydrophilic CC and MDS can effectively promote the conversion of FW to IW and reduce the content of FW, thus inhibiting water activity.^{36, 37} The contact angles of two hydrogel electrolytes were measured to reveal their hydrophilicity (Fig. S10†), where SC-PAM shows a lower water contact angle of 59° than that of PAM (84°). This result confirms the efficacy of enhanced hydration in SC-PAM hydrogel through the incorporation of the strong electronegative carboxyl groups in carboxylated chitosan, which is beneficial to reducing the reaction activity water to avoid Zn corrosion during the electrochemical process.

Since the major barrier to charge transfer usually arises from the desolvation process of hydrated Zn^{2+} ions, the desolvation behavior of $\text{Zn}(\text{OTf})_2/\text{H}_2\text{O}$, PAM and SC-PAM polyelectrolyte hydrogel electrolytes was further evaluated by calculating the desolvation energy (Fig. S11†). Calculation results show that SC-PAM- $[\text{Zn}(\text{H}_2\text{O})_5\text{OTf}]^+$ has a more negative desolvation energy of -18.51 eV than PAM- $[\text{Zn}(\text{H}_2\text{O})_4\text{OTf}]^+$ (-17.06 eV) and $[\text{Zn}(\text{H}_2\text{O})_6]^{2+}$ (-16.74 eV). Additionally, the thermodynamic stability of the cell is critically influenced by the highest occupied molecular orbital (HOMO) and lowest unoccupied molecular orbital (LUMO) at the electrolyte/Zn anode interface.^{38, 39} Therefore, LUMO and HOMO of H_2O , PAM, CC, and MDS were calculated *via* density-functional theory (DFT) calculations. The LUMO energies of MDS (-3.19 eV) and CC (-1.35 eV) in SC-PAM are much lower than that of H_2O molecule (0.019 eV), indicating that the lower LUMO of SC-PAM inhibits the spontaneous reduction of H_2O molecules (Fig. S12†).⁴⁰

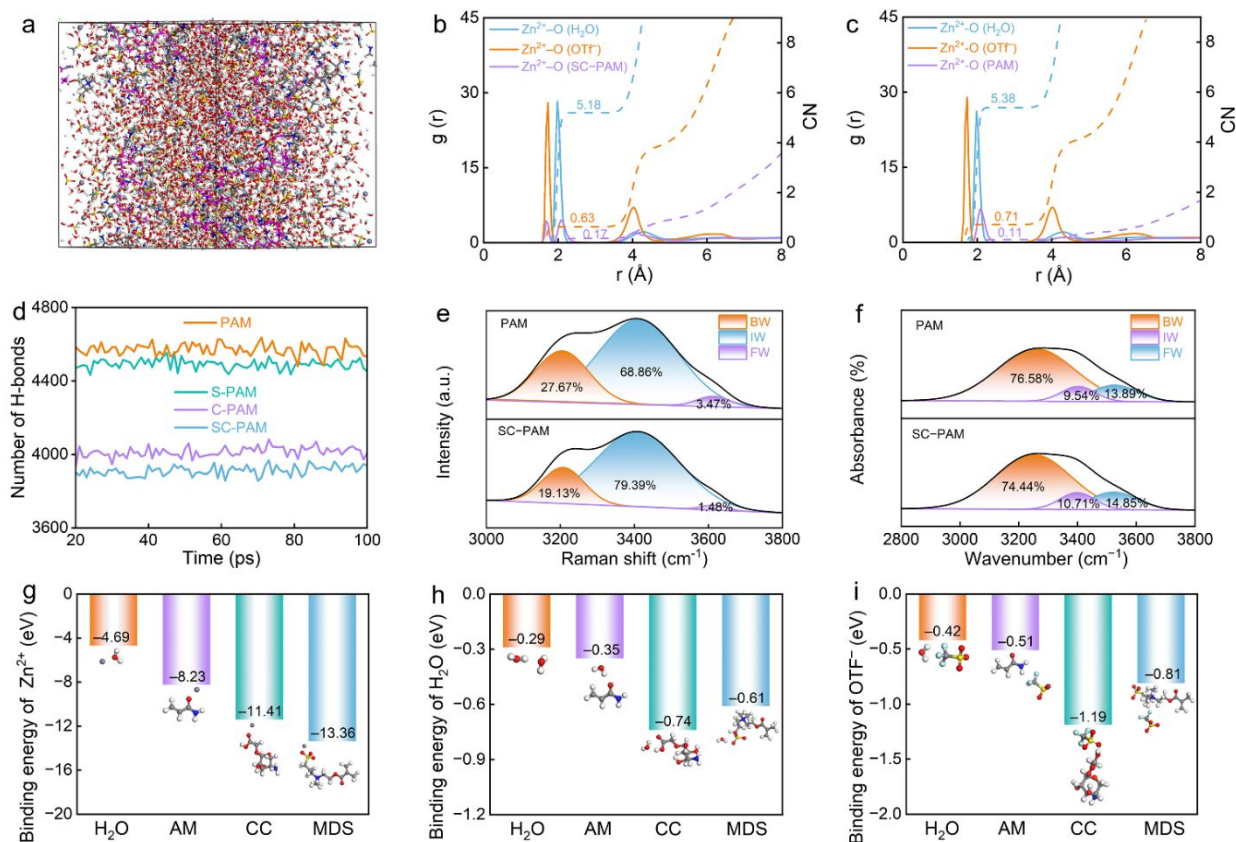


Fig. 3 (a) MD simulation snapshots of SC-PAM and (b, c) RDFs for SC-PAM and PAM. (d) H-bonds number of water molecules in PAM and SC-PAM. (e–f) Raman spectra and FT-IR spectra corresponding Gaussian-Lorentzian fitting. (g–i) Calculated binding energies between Zn^{2+} , H_2O and OTf^- and H_2O , PAM, CC, and MDS.



In SC-PAM, the carboxyl groups of CC and sulfonate groups of MDS exhibit higher theoretical adsorption energies for Zn^{2+} than water (Fig. 3g). An abundance of $-\text{SO}_3^-$ and $-\text{C}=\text{O}$ zincophilic groups in SC-PAM forms an even larger number of lower electronegativity regions, indicating that $-\text{SO}_3^-$ and $-\text{C}=\text{O}$ groups on SC-PAM readily interact with Zn^{2+} . Moreover, calculated binding energies between electrolyte components and both water molecules/anionic groups show that the formation energies of $\text{CC-H}_2\text{O}$ and $\text{MDS-H}_2\text{O}$ are more negative than that of $\text{H}_2\text{O-H}_2\text{O}$, suggesting that the water molecules tended to interact with the oxygen-containing groups of CC and MDS, thus breaking the inherent H-bonding network between $\text{H}_2\text{O-H}_2\text{O}$ (Fig. 3h and i).^{41, 42} Moreover, after the introduction of SC-PAM into the solvation structure, the electrostatic potential of Zn^{2+} solvation structure significantly decreases. As a result, the electrostatic repulsion between Zn cations is reduced, which facilitates the rapid

transport of Zn^{2+} ions (Fig. S13†).^{43, 44} In summary, computational results indicate that both Zn^{2+} and H_2O in SC-PAM prefer to couple with CC and MDS, which breaks the intrinsic H-bonding between free water and regulates the solvated structure of Zn^{2+} ions.⁴⁵

$\text{Zn}||\text{Cu}$ cell using SC-PAM polyelectrolyte hydrogel electrolyte exhibits a lower nucleation overpotential (160 mV) than PAM (540 mV), according to the voltage-capacity curves (Fig. S14†). This result implies fine particles of Zn deposition and homogeneous ions transport (Fig. 4a), as also confirmed by cyclic voltammetry (CV). No other peaks in CV profiles can be observed over the voltage window from -0.4 and 0.4 V for Zn plating/stripping, indicating good stability of SC-PAM.^{46, 47} As evaluated by Tafel test, the Zn anode in SC-PAM demonstrates the lowest corrosion current of 0.149 mA cm^{-2} (Fig. 4b) in comparison with S-PAM (0.424 mA cm^{-2}), C-PAM (0.188 mA cm^{-2}), and PAM (0.479 mA cm^{-2}). In addition, the Zn^{2+}

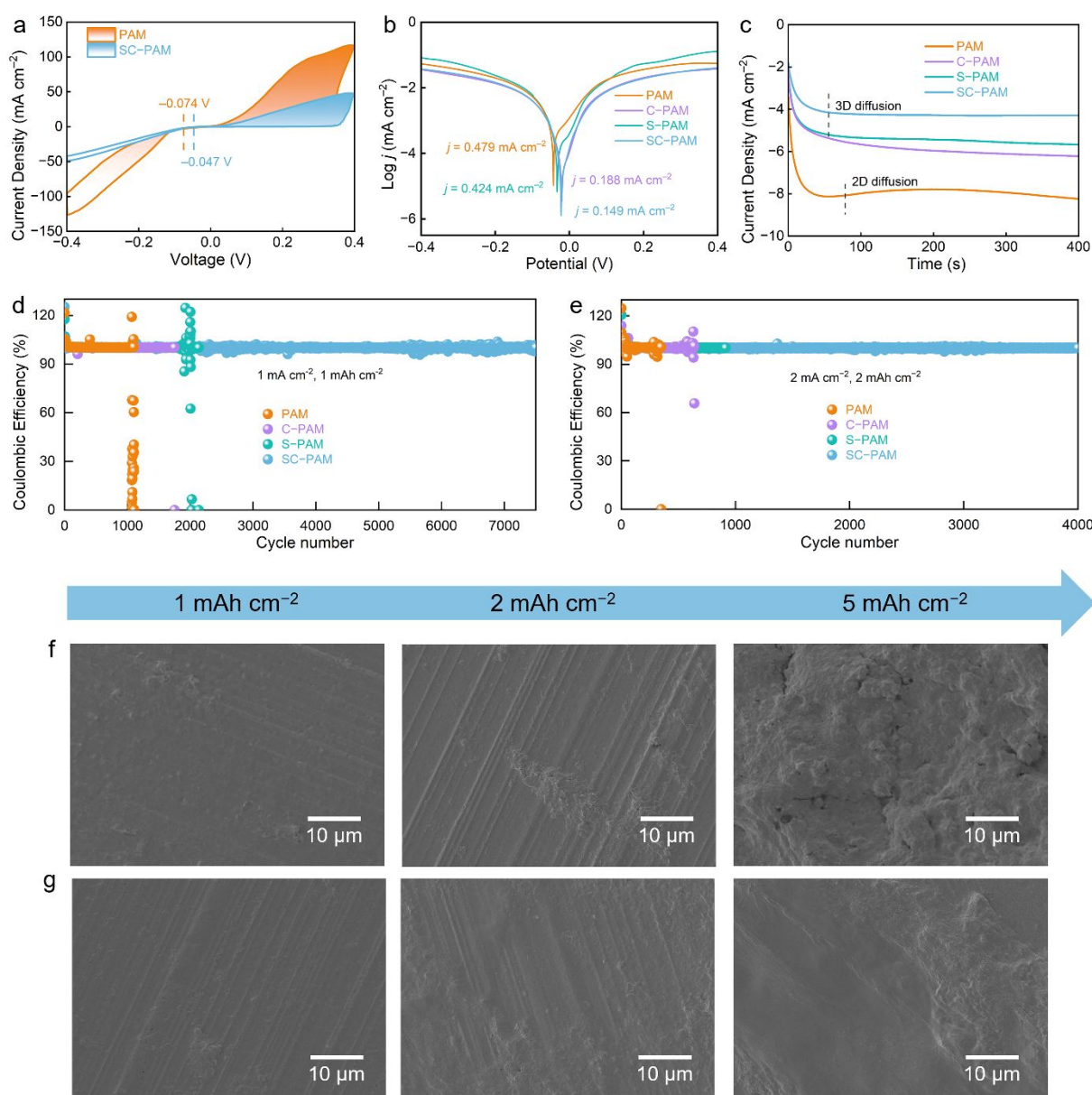


Fig. 4 (a) Cyclic voltammograms of $\text{Zn}||\text{Cu}$ cells using PAM and SC-PAM hydrogel electrolytes at 1 mV s^{-1} . (b) Tafel plots. (c) CA test of $\text{Zn}||\text{Zn}$ cells at a constant voltage of -150 mV . (d-e) Long-term performance of $\text{Zn}||\text{Cu}$ cells. SEM images of plating Zn on Cu current collector with different areal capacities in (f) PAM and (g) SC-PAM.



nucleation and growth behavior on the Zn anode surface in different hydrogel electrolytes were tested by CA curves with a fixed voltage of -150 mV (Fig. 4c). For PAM, the continuous increase in current density within 300 s indicates that the expansion of effective surface area during nucleation leads to uncontrolled diffusion, which hinders the uniform Zn^{2+} nucleation. In contrary, the current density for SC-PAM becomes stable rapidly. This phenomenon is related to the interface protective layer formed on the Zn anode surface, which provides sufficient nucleation sites and induces the unique three-dimensional diffusion of Zn^{2+} , which is beneficial for uniform Zn deposition and can effectively alleviate Zn dendrite formation.⁴⁸

Coulombic efficiency (CE) serves as a key metric for assessing the reversibility of the Zn plating/stripping process. Zn||Cu cell using SC-PAM polyzwitterionic hydrogel electrolyte achieves a higher average CE of 99.6% compared to PAM of 86.6%, which is attributed to the effective suppression of parasitic reactions (Fig. S15†). Remarkably, Zn||SC-PAM||Cu cell exhibits exceptional long-term stability over 7500 cycles, which delivers a high average CE of 99.7% and smooth voltage profiles (Fig. 4d). Conversely, Zn||Cu cell using PAM hydrogel electrolyte exhibits a significantly shortened cycle life of 1900 cycles, accompanied by a low average CE of 87.9%. This conclusion is further supported by the evolution of Zn deposition morphology, as observed in SEM images (Fig. 4f and g). With the deposition capacity increasing from 1 to 5 mAh cm^{-2} , the Zn anode morphology evolved into vertically oriented flakes (Fig. 4f), the morphology characteristic of a typical two-dimensional diffusion process as inferred from the CA results (Fig. 4c). By contrast, a densely compact and uniformly distributed Zn morphology is achieved in SC-PAM polyzwitterionic hydrogel electrolyte, originating from the parallel stacking and horizontally oriented growth of individual zinc platelets (Fig. 4g). For comparison, we directly coated electronegative chitosan onto the surface of Zn anode (Fig. S16†), showing limited efficacy in inhibiting Zn dendrites and corrosion compared to polyzwitterionic SC-PAM hydrogel electrolyte. These observations demonstrate the effective regulation capability of SC-PAM polyzwitterionic hydrogel electrolyte on Zn nucleation and growth processes.^{49, 50}

Zn||SC-PAM||Zn symmetric cells can withstand large current density fluctuations and exhibit stable and small overpotential with the increased current densities covering a range between 0.1 and 10 mA cm^{-2} (Fig. 5a). Noteworthy, a slight reduction in polarization voltage was observed for the Zn||SC-PAM||Zn cell at a reset current density of 0.2 mA cm^{-2} compared to the initial value. After cycling at different current densities, we conducted cycle testing of the battery, which demonstrated excellent cycle stability (Fig. S17†). In contrast, Zn||PAM||Zn cell suffers from a short circuit at 10 mA cm^{-2} due to severe dendrites. This further demonstrates the superior rate capability and cycling stability of Zn||SC-PAM||Zn cell. To evaluate the long-term practical potential, the shelf life and recyclability of Zn||SC-PAM||Zn batteries by intermittent galvanostatic (dis)charge test at 0.5 mA cm^{-2} /mAh cm^{-2} (Fig. 5b). The cell maintains an impressive cycling stability over 1200 hours, demonstrating a high stability during (dis)charging.^{51, 52}

Zn||SC-PAM||Zn cell delivers an overpotential below 100 mV without obvious voltage polarization and continues (dis)charging duration over 7500 h at 0.5 mA cm^{-2} /mAh cm^{-2} , indicating stable Zn

plating/stripping process. While Zn||PAM||Zn cells only maintains 550 h at 0.5 mA cm^{-2} , accompanied by fast short currents (Fig. 5c and d). Compared with PAM, polyzwitterionic SC-PAM hydrogel electrolyte affords better electrochemical stability for Zn||Zn cells due to its highly zincophilic-hydrophobic properties. The zincophilic $-\text{SO}_3^-$ motifs of sulfobetaine in SC-PAM afford highly Zn^{2+} -selective migration channels to homogenize Zn^{2+} flux. Meanwhile, strong electronegative C=O groups in chitosan strongly anchor H_2O molecules via rich H-bonds to form hydrophobic interfacial layers, which shield direct contact between H_2O solvent and Zn anode to avoid Zn corrosion. The formation of Zn dendrites and passivation between the PAM hydrogel electrolyte and Zn anode are the primary factors leading to cell failure. Moreover, Zn||SC-PAM||Zn cell exhibits a low overpotential of 450 mV and cycling stability at 1 mA cm^{-2} /mAh cm^{-2} . Besides, to evaluate the application potential of SC-PAM in high energy devices with high depth of discharge (DOD), Zn||SC-PAM||Zn cell was performed with the different levels of (dis)charging measurements employing a 10 μm -thick Zn foil. The polarization voltage of Zn||SC-PAM||Zn cell exhibits high stability with the DOD of 30% and 50% (Fig. 5e and Fig. S18†).

The influence of SC-PAM on the Zn deposition morphology was further investigated by SEM image observation. The Zn electrode surface in Zn||PAM||Zn cell is uneven and consists of flaky agglomerates after 100 cycles (Fig. 5f). On the contrary, the deposition morphology of Zn electrode in Zn||SC-PAM||Zn cell is flat and smooth without obvious protrusions (Fig. 5g). This result proves that SC-PAM effectively induces the homogeneous Zn deposition based on electrostatic adsorption, thus effectively suppressing the formation of dendritic protrusions and Zn corrosion and prolonging the electrochemical stability of the Zn anode.⁵³

To further investigate the effect of SC-PAM on ion regulation, XRD patterns of Zn anode in Zn||Zn cells after cycling were analyzed. The intensity ratio of the diffraction peaks between Zn (002) and (101) indicates that Zn^{2+} ions tend to deposit on the (002) plane of Zn anode in Zn||SC-PAM||Zn cell, which usually results in a flat Zn anode surface (Fig. 5h).⁵⁴ In addition, the Zn anode in Zn||SC-PAM||Zn cell shows diffraction peaks similar to those of pure Zn foil, whereas the Zn anode of PAM-based cells shows diffraction peaks related to by-products. By-products typically result in the creation of cavities and passivation on the Zn anode surface.⁵⁵ Furthermore, we tested XRD patterns on the Zn anode surface of Zn||SC-PAM||Zn cell after 500, 1000, 1500, and 2000 h cycling. The relative peak intensity ratio of the (002) plane to the (101) plane gradually increases with the increase in the cycling time (Fig. S19†). It can be seen that the (002) plane becomes the main deposition crystal plane after 500 h cycling, which indicates the preferential orientation of Zn deposition plane.^{56, 57}

To elaborate the mechanism of SC-PAM polyzwitterionic hydrogel electrolyte on Zn deposition behavior, the adsorption energies of H_2O , PAM and SC-PAM on different Zn crystal planes were computed via DFT calculations. The results reveal that SC-PAM exhibits significantly stronger adsorption on both (002) and (101) Zn planes (with energies of -1.44 eV and -1.68 eV, respectively) compared to H_2O (-0.32 eV and -0.28 eV) (Fig. 5i). Thus, the preferential adsorption of SC-PAM on the Zn surface regulates the electric double layer and forms a hydrophobic environment, thereby achieving effective anti-corrosion.⁵⁸ The slowest Zn^{2+} deposition rate



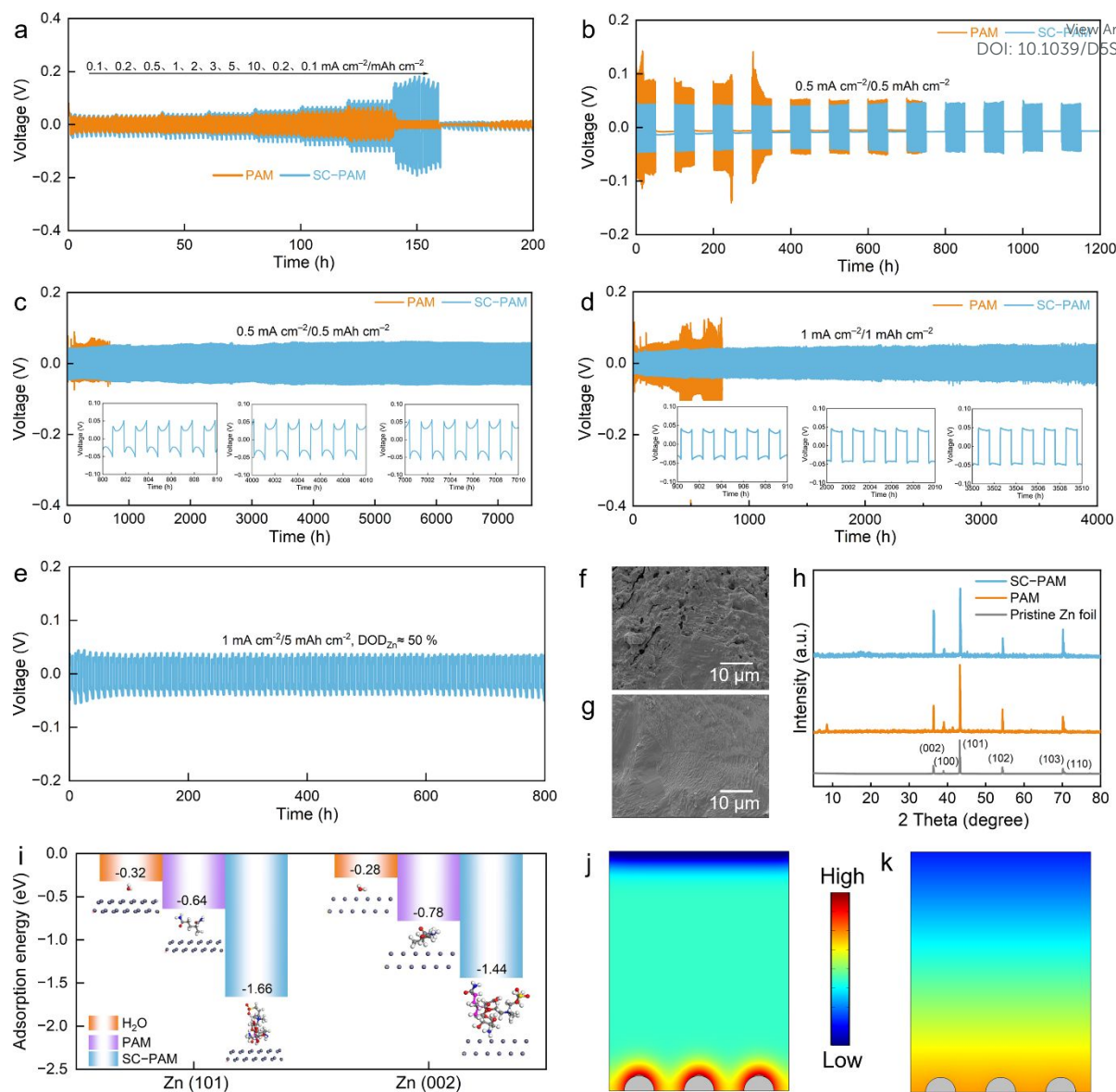


Fig. 5 (a) Voltage profiles of Zn||Zn cells. (b) Cycling performance of Zn||Zn cells during intermittent galvanostatic charge/discharge test at 0.5 mA cm⁻²/0.5 mAh cm⁻². Voltage profiles of Zn||Zn cells at (c) 0.5 mA cm⁻²/0.5 mAh cm⁻², (d) 1 mA cm⁻²/1 mAh cm⁻², and (e) 1 mA cm⁻²/5 mAh cm⁻². SEM images of the Zn electrodes after 100 cycles at 1 mA cm⁻² using (f) PAM and (g) SC-PAM. (h) XRD patterns of Zn electrodes after cycling. (i) Adsorption energy of H₂O, PAM and SC-PAM on (002) and (101) crystal planes of Zn. COMSOL simulations of the Zn²⁺ flux distributions of Zn electrode with (j) PAM and (k) SC-PAM.

occurs along the (101) Zn planes due to electrostatic repulsion. This is driven by the preferential adsorption of SC-PAM on (101) plane (-1.68 eV), which exhibits a stronger interaction than (002) plane (-1.44 eV). Such a feature promotes the exposure of (002) plane and the formation of preferred (002) deposition textures. This hydrophobic layer can modulate the interfacial ion distribution, eliminate tip effects, and form a water-blocking barrier to mitigate the Zn corrosion.⁵⁹

Besides, COMSOL simulations of the Zn²⁺ flux distributions of Zn electrode confirm that the positive effect of SC-PAM on improving zinc deposition behavior. PAM hydrogel electrolyte exhibits an uneven electric field distribution during the initial nucleation stage to trigger the "tip effect", which results in excessive Zn deposition at protrusions and the formation of sharp dendrites (Fig. 5j). While SC-PAM polyelectrolyte hydrogel electrolyte regulates Zn²⁺ ions flux

and homogenizes the interfacial electric field distribution (Fig. 5k), enabling the uniform distribution of initial zinc nuclear on the electrode surface and thus ensuring subsequent stable zinc deposition.^{60, 61}

To evaluate the application prospects of SC-PAM polyelectrolyte hydrogel electrolyte, modified V₂O₅ materials (mass loading: ~1.2 mg cm⁻²) was acted as the cathode to couple with Zn foil anode to construct Zn||SC-PAM||V₂O₅ cell. CV curves of the battery shows two pairs of peaks at 0.1–1.0 mV s⁻¹ covering a range from 0.2 to 1.6 V (Fig. 6a). The dominant role of surface capacitive behavior in the charge storage mechanism is evidenced by the high *b*-values,⁶² which corresponds to rapid ion diffusion (Fig. 6b). Such a result suggests that the redox process involves both diffusion- and capacitive-controlled steps.⁶³ The rapid capacitive contribution of V₂O₅ cathode at a scan rate of 1 mV s⁻¹ was quantitatively evaluated,



demonstrating a high proportion of 93.43% (Fig. 6c). As the scan rate increases, the capacitive contribution from fast surface-redox reactions dominates that of the diffusion-controlled process, rising from 73.03% to 93.43% (Fig. 6d). These results confirm the superior energy storage kinetics of V_2O_5 cathode. The self-discharge behavior of polyelectrolytic SC-PAM hydrogel electrolyte was investigated at the fully charged state of 1.6 V at 0.2 A g^{-1} (Fig. S20†). After standing for 24 hours, the coulombic efficiency of SC-PAM hydrogel electrolyte is as high as 95% compared to PAM (85%). Such a result indicates the desirable structural stability and practical applicability of SC-PAM hydrogel electrolyte in $Zn||SC-PAM||V_2O_5$ battery.

$Zn||SC-PAM||V_2O_5$ shows a specific discharge capacity of 372 mAh g^{-1} at 0.1 A g^{-1} . The specific capacities of $Zn||SC-PAM||V_2O_5$ are 372, 352, 323, 299, 280, 265, 230, 216, 189 and 168 mAh g^{-1} at

0.2, 0.3, 0.5, 1, 2, 3, 5, 10 and 15 A g^{-1} respectively. The excellent rate capability is demonstrated by the highly reversible capacity, which specific capacities recovers to 371 mAh g^{-1} when the current was reset to 0.1 A g^{-1} .⁶⁴ The constant current charge-discharge (GCD) curves of $Zn||SC-PAM||V_2O_5$ cell exhibits high capacities (Fig. 6f), owing to the unique polyelectrolytic structure of SC-PAM. Besides, the battery delivers a superior capacity of 353 mAh g^{-1} after 5000 cycles at 0.2 A g^{-1} (Fig. 6g). V_2O_5 cathode shows identical XRD patterns before and after long-term cycling (Fig. S21†), suggesting its unchanged crystal structure during the continuous electrochemical process. Notably, even under a high current density of 2 A g^{-1} , $Zn||SC-PAM||V_2O_5$ cell still maintains 99% CE and 84.9% capacity retention after 2000 cycles (Fig. 6h), indicating its outstanding electrochemical cycling stability.

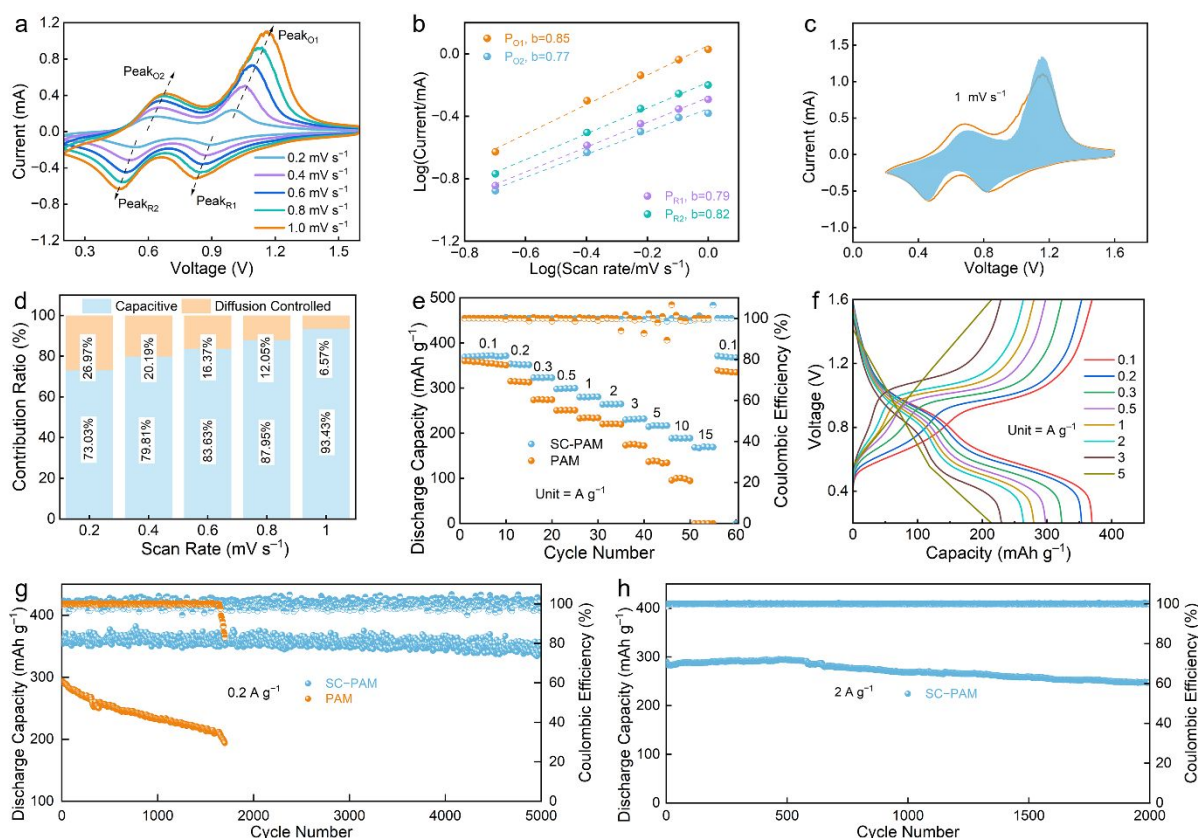


Fig. 6 Charge storage kinetics of $Zn||SC-PAM||V_2O_5$ cell. (a) CV curves. (b) Calculated b values. (c) Capacitive contribution at 1 mV s^{-1} . (d) Ratios of capacitive and diffusion-controlled contribution at various scan rates. (e) Rate performance. (f) GCD curves. Long-term cycling performance at (g) 0.2 A g^{-1} and (h) 2 A g^{-1} .

Conclusion

In conclusion, a highly zincophilic-hydrophobic polyelectrolytic hydrogel electrolyte is designed by the crosslinking of strong electronegative zwitterionic sulfobetaine and carboxyl-rich carboxylated chitosan, to regulate uniform Zn^{2+} conduction and suppress Zn corrosion for stabilized Zn anode. The zincophilic $-SO_3^-$ units of zwitterionic sulfobetaine in SC-PAM provide highly Zn^{2+} -selective diffusion pathways and homogenize Zn^{2+} deposition with a high transference number of 0.90. Meanwhile, electronegative carboxylated chitosan form a hydrophobic interface on Zn anode through H-bonding interactions to shield direct contact between H_2O solvent and Zn anode, thereby inhibiting water-induced corrosion. As

a consequence, SC-PAM hydrogel electrolyte endows $Zn||Cu$ cell with 7600 cycles and a high average CE of 99.7%, and $Zn||Zn$ cell with 7500 h duration at 1 mA cm^{-2} . Furthermore, the assembled $Zn||SC-PAM||V_2O_5$ full cell delivers high capacity, high-rate performance, and long lifespan. These findings extend the design concept of zincophilic-hydrophobic polyelectrolytic hydrogel electrolytes for advanced zinc-ion batteries.

Data availability

The data that support the findings of this study are available on request from the corresponding author, upon reasonable request.



Author contributions

M.X.L. conceived the project. L.H.G., and Z.Y.S. supervised the research. J.Z., and Z.Y.S. prepare materials, characterize and analyze the data. Q.H. performed computational simulation. Y.K.L. assisted in conducting electrochemical analysis. J.Z., and Z.Y.S. wrote the paper. All authors engaged in discussions related to the manuscript.

Conflicts of interest

The authors declare no conflict of interest.

Acknowledgements

This work is financially supported by the National Natural Science Foundation of China (No. 22272118, 22172111, and 22309134), the Shanghai Rising-Star Program (23YF1449200), the Zhejiang Provincial Science and Technology Project (2022C01182), and the Fundamental Research Funds for the Central Universities.

Notes and References

- D. Larcher, J. M. Tarascon, *Nat. Chem.* 2015, **7**, 19.
- A. Innocenti, D. Bresser, J. Garche, S. Passerini, *Nat. Commun.* 2024, **15**, 4068.
- Z. Song, W. Liu, Q. Huang, Y. Lv, L. Gan, M. Liu, *Chem. Sci.* 2025, **16**, 16542.
- G. Luderer, S. Madeddu, L. Merfort, F. Ueckerdt, M. Pehl, R. Pietzcker, M. Rottoli, F. Schreyer, N. Bauer, L. Baumstark, C. Bertram, A. Dirnaichner, F. Humpenöder, A. Levesque, A. Popp, R. Rodrigues, J. Streifer, E. Kriegler, *Nat. Energy* 2022, **7**, 380.
- M. Munjal, T. Prein, M. M. Ramadan, H. B. Smith, V. Venugopal, J. L. M. Rupp, I. Abate, E. A. Olivetti and K. J. Huang, *Joule*, 2025, **9**, 101871.
- W. Yang, Y. Yang, H. Yang, H. Zhou, *ACS Energy Lett.* 2022, **7**, 2515.
- Y. Zhang, Y. Fu, Y. Lv, Z. Song, L. Gan, M. Liu, *Chem. Commun.* 2025, **61**, 14611.
- J. Han, A. Mariani, S. Passerini, A. Varzi, *Energ Environ. Sci.* 2023, **16**, 1480.
- X. Zhao, X. Liang, Y. Li, Q. Chen, M. Chen, *Energy Storage Mater.* 2021, **42**, 533.
- S. Lee, J. Hwang, W. Song, S. Park, *Batteries Supercaps* 2022, **5**, e202200237.
- H. Li, J. Hao, S. Qiao, *Adv. Mater.* 2024, **36**, 2411991.
- C. Liu, X. Xie, B. Lu, J. Zhou, S. Liang, *ACS Energy Lett.* 2021, **6**, 1015.
- O. Borodin, J. Self, K. Persson, C. Wang, K. Xu, *Joule* 2020, **4**, 69.
- W. Du, Q. Huang, Y. Lv, Z. Song, L. Gan, M. Liu, *Energ Environ. Sci.* 2025, DOI: 10.1039/D5EE04802H.
- K. Wu, J. Huang, J. Yi, X. Liu, Y. Liu, Y. Wang, J. Zhang, Y. Xia, *Adv. Energy Mater.* 2020, **10**, 1903977.
- D. Mecerreyes, N. Casado, I. Villaluenga, M. Forsyth, *Macromolecules* 2024, **57**, 3013.
- R. Wang, M. Yao, S. Huang, J. Tian, Z. Niu, *Adv. Funct. Mater.* 2021, **31**, 2009209.
- Y. Lv, Y. Xiao, L. Ma, C. Zhi, S. Chen, *Adv. Mater.* 2021, **34**, 2106409.
- H. Zhang, X. Gan, Y. Gao, H. Wu, Z. Song, J. Zhou, *Adv. Mater.* 2024, **37**, 2411997.
- Y.-H. Lee, Y. Jeoun, J. Kim, J. Shim, K.-S. Ahn, S.-H. Yu, Y.-E. Sung, *Adv. Funct. Mater.* 2023, **34**, 2310884.
- P. Jaumaux, S. Wang, S. Zhao, B. Sun, G. Wang, *Energy Environ. Mater.* 2023, **6**, e12578.
- M. Peng, X. Tang, K. Xiao, T. Hu, K. Yuan, Y. Chen, *Angew. Chem. Int. Ed.* 2023, **62**, e202302701.
- Y. Cheng, Y. Jiao, P. Wu, *Energ Environ. Sci.* 2023, **16**, 4561.
- Y. Lei, F. Liu, L. Chen, M. Xu, Y. Hu, T. Abdiryim, F. Xu, J. You, Y. Tan, Z. Tan, X. Liu, *Nano Energy* 2025, **143**, 111284. DOI: 10.1039/D5SC08853D
- J. Yang, J. Li, J. Zhao, K. Liu, P. Yang, H. Fan, *Adv. Mater.* 2022, **34**, 2202382.
- K. Leng, G. Li, J. Guo, X. Zhang, A. Wang, X. Liu, J. Luo, *Adv. Funct. Mater.* 2020, **30**, 2001317.
- Q. Fu, S. Hao, X. Zhang, H. Zhao, F. Xu, J. Yang, *Energ Environ. Sci.* 2023, **16**, 1291.
- L. Mi, S. Jiang, *Angew. Chem. Int. Ed.* 2014, **53**, 1746.
- R. Chen, Q. Liu, L. Xu, X. Zuo, F. Liu, J. Zhang, X. Zhou, L. Mai, *ACS Energy Lett.* 2022, **7**, 1719.
- S. Zhang, H. Ao, J. Dong, D. Wang, C. Wang, X. Xu, Z. Hou, J. Yang, *Angew. Chem. Int. Ed.* 2024, **64**, e202414702.
- T. Kang, J. Lee, J. Lee, J. Park, J. Shin, J. Ju, H. Lee, S. Lee, J. Kim, *Adv. Mater.* 2023, **35**, 2301308.
- W. Zhang, F. Guo, H. Mi, Z. Wu, C. Ji, C. Yang, J. Qiu, *Adv. Energy Mater.* 2022, **12**, 2202219.
- O. Zhanadilov, H. Kim, H. Lai, J. Jiang, A. Konarov, A. Mentbayeva, Z. Bakenov, K. Sohn, P. Kaghazchi, S. Myung, *Small* 2023, **19**, 2302973.
- T. Wu, C. Ji, H. Mi, F. Guo, G. Guo, B. Zhang, M. Wu, *J. Mater. Chem. A* 2022, **10**, 25701.
- Y. Qin, C. Hu, Q. Huang, Y. Lv, Z. Song, L. Gan, M. Liu, *Nano-Micro Lett.* 2026, **18**, 38.
- Z. Shen, Y. Liu, Z. Li, Z. Tang, J. Pu, L. Luo, Y. Ji, J. Xie, Z. Shu, Y. Yao, N. Zhang, G. Hong, *Adv. Funct. Mater.* 2024, **35**, 2406620.
- Q. He, Z. Chang, Y. Zhong, S. Chai, C. Fu, S. Liang, G. Fang, A. Pan, *ACS Energy Lett.* 2023, **8**, 5253.
- S. Cui, W. Miao, X. Wang, K. Sun, H. Peng, G. Ma, *ACS Nano* 2024, **18**, 12355.
- H. Lu, J. Hu, X. Wei, K. Zhang, X. Xiao, J. Zhao, Q. Hu, J. Yu, G. Zhou, B. Xu, *Nat. Commun.* 2023, **14**, 4435.
- X. Wang, W. Zhou, L. Wang, Y. Zhang, S. Li, X. Li, Z. Zhao, T. Zhang, H. Jin, X. Song, P. Liang, B. Zhang, D. Zhao, D. Chao, *Adv. Mater.* 2025, **37**, 2501049.
- Y. Zhang, X. Zheng, N. Wang, W. Lai, Y. Liu, S. Chou, H. Liu, S. Dou, Y. Wang, *Chem. Sci.* 2022, **13**, 14246.
- X. Yang, Z. Zhang, M. Wu, Z. Guo, Z. Zheng, *Adv. Mater.* 2023, **35**, 2303550.
- A. Khayum M, M. Ghosh, V. Vijayakumar, A. Halder, M. Nurhuda, S. Kumar, M. Addicoat, S. Kurungot, R. Banerjee, *Chem. Sci.* 2019, **10**, 8889.
- J. Ke, Z. Wen, Y. Yang, R. Tang, Y. Tang, M. Ye, X. Liu, Y. Zhang, C. Li, *Adv. Funct. Mater.* 2023, **33**, 2301129.
- Y. Wang, Q. Li, H. Hong, S. Yang, R. Zhang, X. Wang, X. Jin, B. Xiong, S. Bai, C. Zhi, *Nat. Commun.* 2023, **14**, 3890.
- G. Gao, X. Huo, B. Li, J. Bi, Z. Zhou, Z. Du, W. Ai, W. Huang, *Energ Environ. Sci.* 2024, **17**, 7850.
- G. Li, Z. Zhao, S. Zhang, L. Sun, M. Li, J. Yuwono, J. Mao, J. Hao, J. Vongsivut, L. Xing, C. Zhao, Z. Guo, *Nat. Commun.* 2023, **14**, 6526.
- B. Li, S. Liu, Y. Geng, C. Mao, L. Dai, L. Wang, S. Jun, B. Lu, Z. He, J. Zhou, *Adv. Funct. Mater.* 2023, **34**, 2214033.
- Z. Song, J. Ding, B. Liu, X. Liu, X. Han, Y. Deng, W. Hu, C. Zhong, *Adv. Mater.* 2020, **32**, 1908127.
- X. Hu, H. Dong, N. Gao, T. Wang, H. He, X. Gao, Y. Dai, Y. Liu, D. Brett, I. Parkin, G. He, *Nat. Commun.* 2025, **16**, 2316.
- Z. Chen, X. Li, D. Wang, Q. Yang, L. Ma, Z. Huang, G. Liang, A. Chen, Y. Guo, B. Dong, X. Huang, C. Yang, C. Zhi, *Energ Environ. Sci.* 2021, **14**, 3492.
- S. Yang, Q. Wu, Y. Li, F. Luo, J. Zhang, K. Chen, Y. You, J. Huang, H. Xie, Y. Chen, *Angew. Chem. Int. Ed.* 2024, **63**, e202409160.
- H. Wu, S. Zhang, J. Vongsivut, M. Jaroniec, J. Hao, S. Qiao, *Joule* 2025, **9**, 102000.
- J. Cong, X. Shen, Z. Wen, X. Wang, L. Peng, J. Zeng, J. Zhao, *Energy Storage Mater.* 2021, **35**, 586.



ARTICLE

Journal Name

- 55 X. Li, J. Chen, T. Wang, B. Wang, Y. Cao, D. Chao, Y. Tang, *Angew. Chem. Int. Ed.* 2025, **64**, e202505855.
- 56 D. Zhang, Z. Song, L. Miao, Y. Lv, H. Duan, M. Li, L. Gan, M. Liu, *Angew. Chem. Int. Ed.* 2025, **64**, e202414116.
- 57 X. Wang, B. Wang, P. Lei, X. Wang, L. Zhou, J. Zhang, J. Zhang, J. Cheng, *Energ Environ. Sci.* 2024, **17**, 6640.
- 58 D. Lin, Y. Lin, R. Pan, J. Li, A. Zhu, T. Zhang, K. Liu, D. Feng, K. Liu, Y. Zhou, C. Yang, G. Hong, W. Zhang, *Nano-Micro Lett.* 2025, **17**, 193.
- 59 H. Tian, M. Yao, Y. Guo, Z. Wang, D. Xu, W. Pan, Q. Zhang, *Adv. Energy Mater.* 2024, **15**, 2403683.
- 60 C. Tian, H. Wang, L. Xie, Y. Zhong, Y. Hu, *Adv. Energy Mater.* 2024, **14**, 2400276.
- 61 Y. Dai, W. Du, H. Dong, X. Gao, C. Su, P. Paul, B. Lukic, C. Zhang, C. Ye, J. Li, W. Zong, J. Li, Y. Liu, A. Rack, L. Mai, P. Shearing, G. He, *Nat. Commun.* 2025, **16**, 7312.
- 62 K. Guo, Z. Song, Y. Lv, L. Gan, M. Liu, *Adv. Funct. Mater.* 2025, **35**, 2506036.
- 63 M. Wu, C. Shi, J. Yang, Y. Zong, Y. Chen, Z. Ren, Y. Zhao, Z. Li, W. Zhang, L. Wang, X. Huang, W. Wen, X. Li, X. Ning, X. Ren, D. Zhu, *Adv. Mater.* 2024, **36**, 2310434.
- 64 D. Xu, Y. Wang, H. Tian, Y. Chen, X. Tian, Q. Zhang, *Adv. Energy Mater.* 2025, **15**, 2502217.

View Article Online
DOI: 10.1039/D5SC08853D



The data that support the findings of this study are available on request from the corresponding author, upon reasonable request.

[View Article Online](#)
DOI: 10.1039/D5SC08853D

